The sodium/proton exchanger SLC9C1 (sNHE) is essential for human sperm motility and fertility

Emma Cavarocchi, Marjorie Whitfield, Ahmed Chargui, Laurence Stouvenel, Patrick Lorès, Charles Coutton, Christophe Arnoult, Pietro Santulli, Catherine Patrat, Nicolas Thierry-Mieg, et al.

The sodium/proton exchanger SLC9C1 (sNHE) is essential for human sperm motility and fertility.

Emma Cavarocchi[1], Marjorie Whitfield[1], Ahmed Chargui[2], Laurence Stouvenel[1], Patrick Lorès[1], Charles Coutton[3,4], Christophe Arnoult[3], Pietro Santulli[5], Catherine Patrat[1,2], Nicolas Thierry-Mieg[6], Pierre F. Ray[3,7], Emmanuel Dulioust[1,2], Aminata Touré[3,*].

[1] Université de Paris, Institut Cochin, INSERM, CNRS, F-75014 PARIS, France.

[2] Laboratoire d'Histologie Embryologie - Biologie de la Reproduction - CECOS Groupe Hospitalier Universitaire Paris Centre, Assistance Publique-Hôpitaux de Paris. Paris 75014, France.

[3] Université Grenoble Alpes, Institut pour l'avancée des Biosciences, INSERM, CNRS, F-38000 GRENOBLE, France.

[4] CHU Grenoble Alpes, UM de Génétique Chromosomique, Grenoble, France.

[5] Service de chirurgie gynécologie obstétrique 2 et médecine de la reproduction. Groupe Hospitalier Universitaire Paris Centre, Assistance Publique-Hôpitaux de Paris. Paris 75014, France.

[6] Univ. Grenoble Alpes, CNRS, TIMC-IMAG / BCM, F-38000 Grenoble, France.

[7] CHU de Grenoble, UM GI-DPI, Grenoble, F-38000, France.

[*]Corresponding author: aminata.toure@inserm.fr

Running Title : *SLC9C1* mutation in human asthenozoospermia

Conflict of interest Statement

The authors declare no conflict of interest.

Abstract

Asthenozoospermia, defined by the absence or reduction of sperm motility, constitutes the most frequent cause of human male infertility. This pathological condition is caused by morphological and/or functional defects of the sperm flagellum, which preclude proper sperm progression. While in the last decade many causal genes were identified for asthenozoospermia associated with severe sperm flagellar defects, the causes of purely functional asthenozoospermia are still poorly defined. We describe here the case of an infertile man, displaying asthenozoospermia without major morphological flagellar anomalies and carrying a homozygous splicing mutation in *SLC9C1* (sNHE), which we identified by whole-exome sequencing. *SLC9C1* encodes a sperm-specific sodium/proton exchanger, which in mouse regulates pH homeostasis and interacts with the soluble Adenylyl Cyclase (sAC), a key regulator of the signalling pathways involved in sperm motility and capacitation. We demonstrate by means of RT-PCR, immunodetection and immunofluorescence assays on patient's semen samples that the homozygous splicing mutation (*c.2748+2T>C*) leads to in-frame exon skipping resulting in a deletion in the cyclic nucleotide-binding domain of the protein. Our work shows that in human, similar to mouse, SLC9C1 is required for sperm motility. Overall, we establish a homozygous truncating mutation in *SLC9C1* as a novel cause of human asthenozoospermia and infertility.

Key words: male infertility; asthenozoospermia; gene mutation; whole-exome sequencing; SLC9C1 - sNHE; ion channel.

Graphical abstract

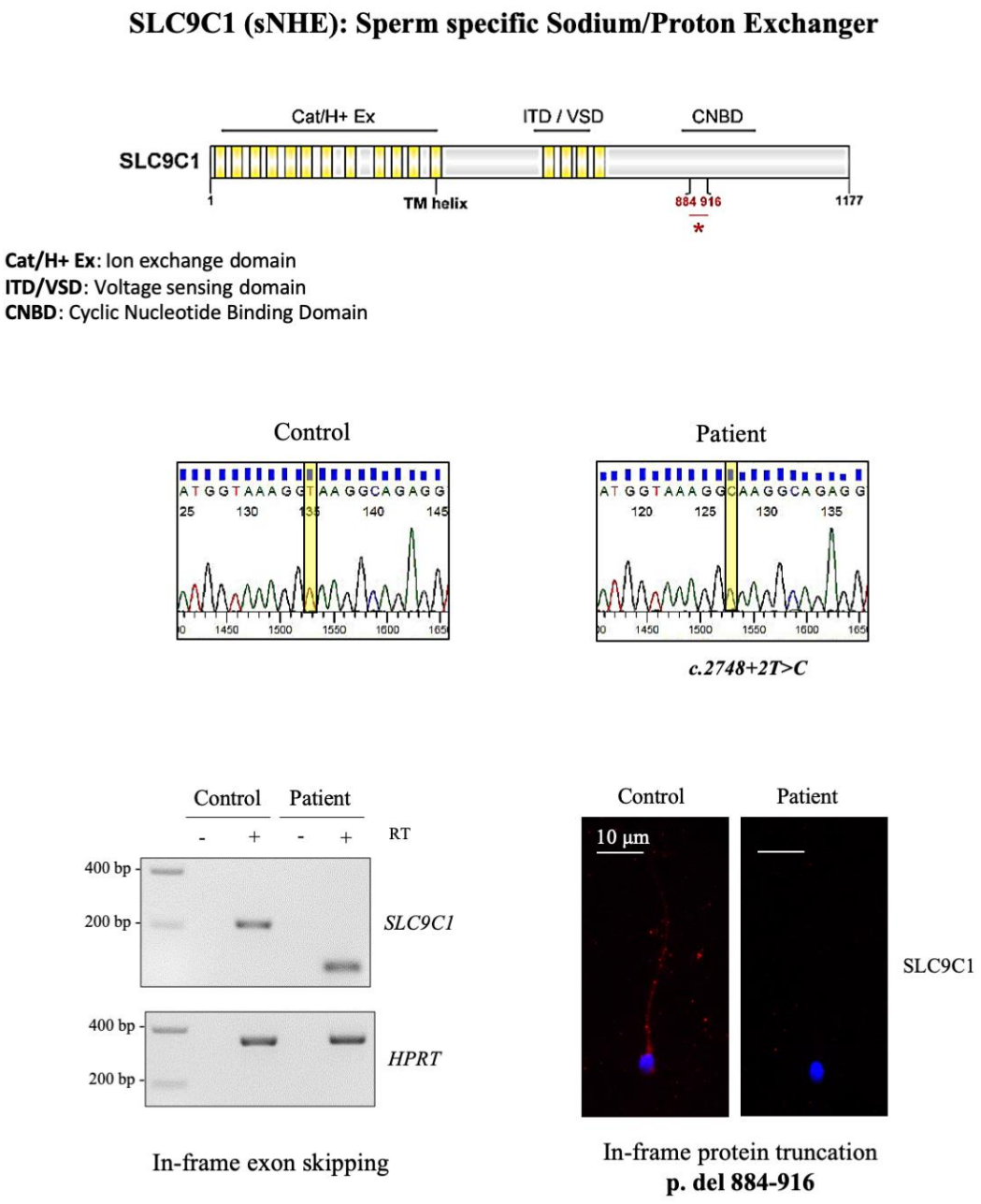

Introduction

Asthenozoospermia, defined by the absence or reduction of sperm motility, is observed in nearly 80% of male infertility cases, either alone or in association with other sperm defects[1]. This pathophysiological condition is induced by structural defects of the sperm flagellum and/or functional alterations impairing flagellar beating and sperm progression. Among the structural defects, a remarkable condition described as Multiple Morphological Abnormalities of sperm Flagella (MMAF) results from defective assembly of the flagellum and leads to the presence in the ejaculate of spermatozoa with short, absent, coiled, bent or irregular tails. This phenotype of asthenoteratozoospermia was previously identified as 'dysplasia of the fibrous sheath', 'short tails' or 'stump tails'[2–4], and in the last decade, numerous mutations causing this phenotype were identified (AK7, ARMC2, MAATS1, CEP135, *CFAP43-44-65-69-70-251*, *DNAH1-2-6-8-17*, *QRICH2*, *SPEF2*, *TTC21A*, *TTC29*)[5,6]. Besides MMAF, some asthenoteratozoospermic patients with milder morphological defects such as defective annulus and abnormal mitochondrial sheath were also described to carry mutations (TEKT2, *SEPT12* or *SLC26A8)*[1,7,8]. Importantly, asthenozoospermia is also detected in the complete absence of morphological defects, suggesting the involvement of functional defects in activation and/or regulation of flagellar beating. To date, such cases of functional asthenozoospermia remain poorly characterized, and only a few mutations were identified in genes encoding for proteins with enzymatic properties (*GALNTL5*), seminal component (*SEMG1*) and ion channels (*CATSPER1-2-ε*, *SLC26A3*, *VDAC2*)[1,9–12]. Overall, the knowledge obtained by studying those sperm pathological phenotypes provides evidence that, in addition to proper morphology and structure, sperm fertilization potential relies on proper activation of the signalling pathways regulating motility, metabolism and energy production.

Sperm functional maturation occurs after spermiation during the transit within the epididymis, where sperm cells acquire the ability to move forward, and ultimately within the

female genital tract, where they acquire complete fertilization potential through a process known as capacitation[13]. Numerous ion channels and transporters have been identified at the surface of sperm cells and conduct complex fluxes between the male and female genital tract milieus and the sperm cytoplasm[14]. These ion exchanges activate several biochemical and electrophysiological changes that are essential for sperm motility and fertilization potential[15]. Among the changes occurring within the female genital tract (i.e. capacitation), were described alkalinization of the cytoplasm, membrane hyperpolarization and protein phosphorylation cascades induced by the activation of soluble adenylate cyclase (sAC) and Protein Kinase A (PKA), which specifically target flagellar components required for sperm fertilization potential[16].

In the present study, by performing Whole-Exome Sequencing (WES) on a patient presenting a very low progressive motility but no detectable ultrastructural defects of the axoneme, we identified a homozygous pathogenic mutation in *SLC9C1*. This gene, also called *sNHE*, encodes a sperm-specific member of the Na^+/H^+ exchanger family involved in the regulation of pH and cell volume in a wide range of tissues[17]. We demonstrate here that *SLC9C1* is critical for human sperm motility and that mutations in *SLC9C1* are a novel cause of human asthenozoospermia.

Materials & methods

Subject and biological samples

The study was approved by the Comité de Protection des Personnes CPP Ile de France III (record number CPP02748) and performed in accordance with ethical guidelines (Declaration of Helsinki). All patient and control individuals included in the study gave their informed consent prior to their inclusion in the study. Semen samples were obtained by masturbation after 2-7 days of sexual abstinence. Semen parameters were evaluated according to the World Health Organization (WHO) guidelines[18] and David's classification[19].

WES analysis and Sanger sequencing

WES analysis was performed on genomic DNA extracted from a blood sample, as previously described[20]. In brief, the enrichment of coding regions together with intron/exon boundaries was performed with Exon V5 kit (Agilent Technologies, Wokingham, UK). Sequencing was performed with Illumina HiSeq 2000 at the Genoscope (Evry, France). Exome-seq data were analysed using a bioinformatics pipeline developed in-house as previously described[21]. The homozygous mutation in *SLC9C1* identified by WES was confirmed by Sanger sequencing using ABI 3130XL and SeqScape software (Applied Biosystems; Foster City, CA, USA). Primer sequences (5'-3'): F: TCCCAACCACTTCTAAAATGTTGT, R: TGCATTTATAAATAACACTGCCTGGT.

Transmission electron microscopy analysis

Sperm cells were collected from fresh ejaculate and washed with M2 medium (Sigma-Aldrich Co. Ltd; Irvine, UK) by centrifugation at 300g/RT for 10 minutes. Sperm cells were then fixed

and embedded for semi-thin sections as previously described[22]. All sections were examined with a JEOL 1011 electron microscope (Jeol Ltd; Tokyo, Japan). Images were acquired with Digital Micrograph software coupled to a Gatan Erlangshen CCD camera.

RT-PCR analysis

Total RNA from control and patient spermatozoa (800-1000ng) was extracted using NucleoSpin RNA kit (Macherey-Nagel; Düren, Germany) and used for reverse transcription with High-Capacity cDNA Reverse Transcription Kit (Applied Biosystems, Thermo Fisher Scientific; Waltham, MA, USA) as previously described[22]. Amplicons were gel purified and sequenced (Eurofins Scientifics, France). Results were analysed with BioEdit software (Ibis Therapeutics; Carlsbad, CA, USA).

Primer sequences (5'-3'): ***SLC9C1*-F**: TTATCAGGCCTCTTACTGTTG, ***SLC9C1*-R**: TGATCAATCCCTAAACCTGGC; ***HPRT*-F**: CCTGCTGGATTACATTAAAGCACTG, ***HPRT*-R**: GTCAAGGGCATATCCAACAACAAAC.

Immunofluorescence assay

Slides were prepared by spreading 10 µL of fresh semen sample onto a Superfrost Plus slide (Menzel Glasbearbeitungswerk, GmbH & Co. KG; Braunschweig, Germany), followed by fixation 10 minutes in PBS 4% paraformaldehyde. Immunostaining was performed as previously described[22], using commercial antibodies, which specificity was not validated.

Primary antibodies : SLC9C1 rabbit polyclonal antibody raised against the central region (Invitrogen PA5-104160; 1:100 dilution); SLC9C1 rabbit polyclonal antibody raised against the C-terminal region (Sigma SAB2106664; 1:100 dilution); mouse monoclonal anti-α-Tubulin

Sigma T9026 (1:500 dilution). Secondary antibodies: goat polyclonal anti-rabbit IgG Alexa Fluor 568 (Invitrogen A-11029; 1:500 dilution) and goat polyclonal anti-mouse IgG Alexa Fluor 488 (Invitrogen A-28175; 1:500 dilution).

Western blot analysis

10 million sperm cells from control individual and patient were washed in M2 medium and next in PBS. Sperm cells were then subjected to sonication (20s on, 60s off, 15 cycles) in RIPA buffer [150 mM NaCl, 1% NP40 (Sigma-Aldrich Co.; St. Louis, MO, USA), 0.5% DOC, 0.1% SDS, 25 mM TrisHCL, cOmplete Protease Inhibitor Cocktail (Roche, Basel, Switzerland)]. Samples were kept on ice for 30 minutes and centrifuged 13000g at 4°C for 15 minutes. The supernatant was collected and denatured in Laemmli sample buffer, prior to SDS-PAGE [8% acrylamide/bisacrylamide (40%, 37.5:1)] and transfer to nitrocellulose membranes. After a blocking step in PBS 0.1% Tween, 5% BSA or milk for SLC9C1 and β-Tubulin detection, respectively, incubation was performed with primary and secondary antibodies. Primary antibodies: rabbit polyclonal anti-SLC9C1 Invitrogen (PA5-104160; 1:500 dilution) and mouse monoclonal anti-β-Tubulin clone AA2 (Sigma 05-661; 1:2500 dilution). Secondary antibodies: rabbit polyclonal anti-mouse Ig coupled to Horse Radish Peroxydase (HRP) (Dako; 1:1000 dilution), swine polyclonal anti-rabbit Ig coupled to HRP (Dako; 1:1000 dilution).

Results

The patient presented in this study first consulted for primary infertility in 2016 at the age of 31, after two years of natural conception failure, and was followed at the reproductive biology centre of the Cochin hospital (Paris, France). Apart from a non-evolutive chronic hepatitis B diagnosed in 2008, no urogenital disease, neither lifestyle factors nor exposures potentially deleterious for fertility were reported. The couple benefited from intra-marital ICSI performed with fresh ejaculated sperm cells but frozen oocytes because the man failed to produce a semen sample on the day of oocytes pick-up of the first ICSI attempt. Seven out of nine of the thawed oocytes were injected and 3 zygotes were observed 18 hours after ICSI. After a prolonged embryo culture, 3 embryos with a good quality, according to the Istanbul consensus 2011 classification[23], were obtained. Embryo transfer scheduled on day 5 was postponed due to a high endometrial thickness; two of the embryos were frozen at day 5 and the third one at day 6. To date, only one thawed embryo was transferred but the resulting pregnancy ended with a miscarriage after 5 weeks and 3 days.

The successive semen analyses performed over 3 years on the patient revealed a severe alteration of sperm progressive motility, which never exceeded 5% (normal value > 32%), contrasting with normal sperm counts and vitality rates (Table 1). The mean percentage of typical spermatozoa was slightly decreased but the patient did not present any sperm abnormalities indicative of a MMAF phenotype (the percentage of spermatozoa with short, absent and irregular calibre of flagella being under the lower reference values[19]) (Table 1). However, semen analyses indicated a significant proportion of spermatozoa with an excess residual cytoplasm and disorganised midpiece with occurrences of plasma membrane lysis (Figure 1A). In addition, flagellar bending was noticed together with some head anomalies (thin head) (Table 1). Acrosomal staining performed with fluorescent peanut agglutinin (PNA) on sperm sample from the patient indicated an intact acrosome on most of the spermatozoa; hence

the rate of PNA negative sperm cells, indicative of premature acrosomal reaction, was 8.8% and 5.4% for control and patient, respectively. The procedure of sperm selection with density gradient centrifugation slightly increased the fraction of progressive spermatozoa (5-25%) but also induced an increase of the number of isolated sperm heads. We found that the percentage of isolated sperm heads remained very low in control samples defined by normal sperm parameters, including morphology according to WHO[19] (1% and 3% before and after selection, respectively), while it significantly increased in patient sample after density gradient centrifugation (2% and 33% before and after selection, respectively). Importantly, we noted that flagellar bending and breaking points on sperm from the patient were not limited to the connective piece but were also present along the flagella (Supplementary Figure S1). Overall, these observations suggested an important fragility of the sperm tail, amplified by the selection procedure.

We performed Transmission Electron Microscopy (TEM) analysis to precisely examine the sperm ultrastructure of the patient. In line with the observations by optic microscopy, we detected the presence of midpiece defects, in particular, an excess of residual cytoplasm around the mitochondrial sheath and plasma membrane fragility illustrated by plasma membrane lysis (Figure 1B). Importantly, no alteration of the axonemal structure was observed in patient's sperm as quantification indicated a percentage of normal transversal sections (9+2 conformation) close to that recorded in semen from control individuals (Patient: 84%; Control mean: 84.5%, n=4). Overall, the patient presented in this study was classified as a case of asthenozoospermia with a severe reduction of the proportion of progressive sperm, membrane and flagellar fragility but no major defects of the sperm flagellum ultra-structure and assembly.

We thus subsequently performed WES analysis of this patient in search for genetic variants potentially involved in the infertility phenotype. After processing and filtering the data, we identified homozygous variants with high predicted impact on the encoded proteins in three

genes: *c.2748+2T>C* in *SLC9C1*, *c.3583C>T* in *ABCB5* and *c.9del* in *ZNF891*. Among those, the variant *c.2748+2T>C* in *SLC9C1* appeared as the best candidate considering the pattern and abundance of expression of the three genes and the frequency of the variants in the population according to public databases (Supplementary Table 1). Indeed, in contrast to the two other candidates, *SLC9C1* was shown to be preferentially expressed in the testis (Illumina Body Map; The Human Protein Atlas database; Reprogenomics Viewer) and the encoded protein was previously detected in human sperm proteome[24] (Supplementary Table 1). The homozygous variant *c.2748+2T>C* identified in *SLC9C1* impairs a consensus sequence of the splice donor site located downstream of exon 22 and was associated with a low allele frequency in the gnomAD database ($4.6x10^{-5}$, chr3:112180562 A>G (GRCh38.p12), rs2007949663-111899409-A-G). The presence of this homozygous variant in the patient was also consistent with the familial history of infertility and the known consanguinity of his parents (cousins). The proband originated from West Africa (Guinea Conakry); he has two brothers, one of them known to be infertile, and two fertile sisters (Figure 2A). In addition, the proband has one cousin who also displays male infertility; as it was not possible to define if the cousin was from maternal or paternal side, this individual is not included in the genealogic tree (Figure 2A). Unfortunately, we could not obtain to biological samples from the family members. In conclusion, considering all the above arguments, we retained the *c.2748+2T>C* variant identified in *SLC9C1* by WES, which we also confirmed by Sanger sequencing on DNA sample from the proband (Figure 2B).

SLC9C1, also known as *sNHE* or *SLC9A10*, is located on chromosome 3 and comprises 29 exons (Figure 2C). Alternative splicing produces five transcript variants, three of which encoding proteins, and among them transcript *SLC9C1-201* encodes for the longer isoform of 135 kDa (Figure 2C). The full SLC9C1 protein isoform comprises the ion exchange domain (Cat/H^+ ex), which is characteristic of SLC9 family members and is generally formed by ten to

twelve transmembrane (TM) helices (Figure 2C). The protein also exhibits a unique C-terminal tail with four additional TM helices showing similarity to a Voltage-Sensing Domain (ITD/VSD) and a consensus sequence for a Cyclic Nucleotide-Binding Domain (CNBD), which is composed of several α-helices and β-sheets and protrudes towards the cytoplasmic side[25,26]. These two latter features are typical of ions channels, which, unlike solute carriers, are not activated by ion gradients but display a more sophisticated regulatory mechanism dependent on the cell status[14].

To investigate the molecular consequence of the mutation identified in *SLC9C1*, we performed RT-PCR analysis on semen sample from control and patient individuals using forward and reverse primers localised in exons 21 and 23, respectively. The PCR amplicon obtained for control individual was observed at the expected size of 217 bp while product amplified from the patient sample was considerably smaller (Figure 2D). The experimental normalization, operated by analysis of the housekeeping gene *HPRT,* did not reveal any difference in *SLC9C1* transcripts amount between the patient and control individual. Sequencing of *SLC9C1* RT-PCR amplicons indicated the total absence of exon 22 in the transcripts from the patient (Figure 2E). This exon encodes for a region included in the Cyclic Nucleotide-Binding Domain (Figure 2C) and comprises 99 bp. Such exon skipping would therefore cause a 33 amino acids in-frame deletion (corresponding to amino acids 884-916). These results confirm the deleterious impact of the identified variant.

We next performed immunofluorescence assays with two antibodies raised against different epitopes of the SLC9C1 protein: a so-called ‘Central antibody’, which recognizes amino-acids 600-750 of the protein, spanning the VSD, upstream from the deletion and a so-called ‘C-Terminal antibody’ targeting amino-acids 882-932, in the CNBD and mainly coinciding with the deleted sequence. We first observed that both antibodies detected the SLC9C1 protein along the sperm flagellum with a signal intensity decreasing towards the tail

end. Importantly, in consistence with RT-PCR data which predicted the deletion of amino acids 884-916, immunofluorescence assays performed with the ‘Central antibody’ marked SLC9C1 protein in spermatozoa from both control and patient samples (Figure 3A), whereas the ‘C-Terminal antibody’ whose epitope largely overlaps with the deleted region only marked the control sperm (Figure 3A).

Lastly, we performed western blot immunodetection from control and patient sperm protein extracts. Using the ‘Central antibody’ we detected a band at the expected molecular weight of the SLC9C1 longer isoform (135 kDa) in both control and patient sperm samples (Figure 3B). Technical limits of the gel electrophoresis did not permit to evidence the small size difference between the normal and the deleted protein but this data firmly confirm the presence of the SLC9C1 truncated protein in sperm cells from the studied patient.

Discussion

In conclusion, we characterize an infertile patient displaying functional asthenozoospermia caused by a homozygous splice mutation in *SLC9C1*, which generates a 33 amino-acid deletion within the Cyclic Nucleotide-Binding Domain (CNBD). This protein domain is considered to be involved in the interaction and reciprocal modulation between SLC9C1 (sNHE) and the soluble Adenylate Cyclase (sAC) in mouse and sea urchin sperm[26,27], the latter being a key element for the regulation of sperm motility and capacitation.

In mice, the disruption of *Nhe-1* did not impact male fertility[28] while disruption of *Slc9c1 (sNhe)* as well as *Nha1* and *Nha2* (single and double conditional KO mice) all resulted in a phenotype of null sperm motility. Interestingly, these phenotypes were significantly rescued by sperm incubation with cAMP analogues, confirming that Na^+/H^+ family members are required for the activation of sperm motility and capacitation through regulation of the cAMP-PKA signalling pathway[25,29]. SLC9C1 (sNHE) was previously described to only localise to the principal piece of the mouse sperm flagellum[25]. Zhang et al.[36] proposed the same localisation in human sperm cells, although the staining was weak and quite heterogeneous. Our immunostaining assays carried out with two different antibodies suggest a distinct flagellar profile in human sperm. Hence, while we detected a prominent localisation of sNHE in the principal piece of murine spermatozoa (Supplementary Figure S2), in human sperm, SLC9C1 was detected along the whole length of the flagellum.

Regarding, the molecular mechanisms of action, it is well established that intracellular pH regulation is fundamental at different steps of sperm maturation and capacitation[30], and Na^+/H^+ exchangers (NHE) play a remarkable role in sperm alkalinisation [31]. SLC9C1 (sNHE) was shown to be required for pH homeostasis and suggested to promote CatSper activation following Slo3-mediated sperm hyperpolarization during mouse sperm capacitation[25,32]. In

humans, to date no information is available regarding sNHE possible implication in sperm pH homeostasis. Some elements have pointed a role of the proton channel Hv1[33,34], although so far, no mutation in *Hv1* were reported in human asthenozoospermia. Our study therefore sheds light on the essential role of sNHE and a likely similar function in pH homeostasis in humans. Importantly, our findings are in line with a recent comparative genomic analysis, which identified the molecular trio sNHE-sAC-CatSper as an evolutionary conserved machinery for the regulation of sperm flagellar beating in Metazoa[35].

The involvement of *SLC9C1* in human sperm physiology has been poorly investigated, and so far only weak evidence was provided regarding its dysfunction in human asthenozoospermia [17,36,37]. The mutation in *SLC9C1* we described here constitutes a solid demonstration of SLC9C1 involvement in the regulation of human sperm motility and fertilization potential. We show that this mutation has a drastic impact on sperm progression; however sperm motility was not totally abrogated as observed in *Slc9c1* KO mouse model[25]. This difference might be explained by the nature of the mutations in those two models; the KO mouse model totally lacks the protein while the patient carries a truncated protein, which could preserve partial functionality. In addition, while in patient sperm we observed flagellar angulation, excess residual cytoplasm and overall a flagellar fragility upon sperm selection, such defects were not reported in the KO mouse model. These observations in patient sperm are compatible with a dysregulation of the ion equilibrium and overall cell volume regulation, which were previously described to depend on channels and aquaporins activity[38].

Overall, this article provides a new evidence of the physiological importance of ion exchange regulation and pH homeostasis in the control of sperm motility and fertilization potential. The first and most remarkable evidence was provided for the CATSPER channel, for which mutations (*CATSPER 1-2-ε* subunits) were identified in several asthenoteratozoospermic individuals with altered fertilizing capacity and/or sperm with coiled flagella[12,39]. More

recently, pathogenic variants affecting members of the SLC26 family of anion exchangers, namely *SLC26A3* and *SLC26A8* (*TAT1)*, were also shown to impair the functionality of the Cystic Fibrosis Transmembrane conductance Regulator (CFTR) channel, causing asthenozoospermia, associated with defective capacitation, midpiece and annulus disorganization in the case of *SLC26A8*[11,40,41]. The voltage-dependent anion channels *VDAC2 and 3* were also identified with pathogenic defects leading to idiopathic asthenozoospermia [42] [9]. The specific location of all those ion channels/transporters at the plasma membrane of sperm cells, constitutes an interesting cellular background for potential therapeutic strategies to improve sperm motility in asthenozoospermic men.

Acknowledgement

We thank all the individuals and their families for their cooperation, as well as all the referring physicians. We thank all the technicians from the *Service de Biologie de la Reproduction* at the Hospital Cochin (Paris) for routine semen sample evaluation (Jacques Bras, Nathalie Chériau, Véronique Hernandorena, Jean-Claude Cambronne and Caroline Villalon). We thank the Cellular Imaging Facility of the Institut Cochin for electron microscopy procedures.

Author's roles

AT designed the study. ED and CP recruited the patient, performed clinical analysis and characterization. AC and PS carried out the ICSI procedure for the patient and his partner. NTM, CC and PR performed exome and bioinformatics analysis. EC did experimental work (RT-PCR, Sequencing, Immunofluorescence, Immunoblotting, MO analysis), data quantification and analysis. AT did TEM analysis. MW, LS and PL contributed in setting up the experimental conditions. EC and AT performed data illustrations. EC and AT analysed the data and wrote the manuscript. MW, AC, PL, CC, CA, PR, NTM, CP and ED did critical reading of the manuscript.

Funding

This work was supported by the Institut National de la Santé et de la Recherche Médicale (INSERM), the Centre National de la Recherche Scientifique (CNRS), the Université Paris Descartes, the University Grenoble-Alpes, the French National Research Agency (Grant MASFLAGELLA ANR-14-CE15-0002 and FLAGEL-OME ANR-19-CE17-0014 to PR, NTM and AT).

Data Availability Statement

The data that support the findings of this study are available from the corresponding author, [AT], upon reasonable request.

References

1 Heidary Z, Saliminejad K, Zaki-Dizaji M, Khorram Khorshid HR. Genetic aspects of idiopathic asthenozoospermia as a cause of male infertility. *Human Fertility* 2018; : 1–10.

2 Chemes HE, Brugo S, Zanchetti F, Carrere C, Lavieri JC. Dysplasia of the fibrous sheath: an ultrastructural defect of human spermatozoa associated with sperm immotility and primary sterility**Supported by grant 0934 from Consejo Nacional de Investigaciones Científicas y Técnicas. *Fertility and Sterility* 1987; **48**: 664–669.

3 Escalier D. Arrest of flagellum morphogenesis with fibrous sheath immaturity of human spermatozoa. *Andrologia* 2006; **38**: 54–60.

4 Escalier D, Albert M. New fibrous sheath anomaly in spermatozoa of men with consanguinity. *Fertility and Sterility* 2006; **86**: 219.e1-219.e9.

5 Nsota Mbango J-F, Coutton C, Arnoult C, Ray PF, Touré A. Genetic causes of male infertility: snapshot on morphological abnormalities of the sperm flagellum. *Basic Clin Androl* 2019; **29**: 2.

6 Touré A, Martinez G, Kherraf Z-E, Cazin C, Beurois J, Arnoult C *et al.* The genetic architecture of morphological abnormalities of the sperm tail. *Hum Genet* 2020. doi:10.1007/s00439-020-02113-x.

7 Touré A, Lhuillier P, Gossen JA, Kuil CW, Lhôte D, Jégou B *et al.* The Testis Anion Transporter 1 (Slc26a8) is required for sperm terminal differentiation and male fertility in the mouse. *Human Molecular Genetics* 2007; **16**: 1783–1793.

8 Kuo Y-C, Lin Y-H, Chen H-I, Wang Y-Y, Chiou Y-W, Lin H-H *et al. SEPT12* mutations cause male infertility with defective sperm annulus. *Hum Mutat* 2012; **33**: 710–719.

9 Xu A, Hua Y, Zhang J, Chen W, Zhao K, Xi W *et al.* Abnormal Hypermethylation of the VDAC2 Promoter is a Potential Cause of Idiopathic Asthenospermia in Men. *Sci Rep* 2016; **6**: 37836.

10 Ray PF, Toure A, Metzler-Guillemain C, Mitchell MJ, Arnoult C, Coutton C. Genetic abnormalities leading to qualitative defects of sperm morphology or function: Genetic abnormalities leading to qualitative sperm defects. *Clin Genet* 2017; **91**: 217–232.

11 Touré A. Importance of SLC26 Transmembrane Anion Exchangers in Sperm Post-testicular Maturation and Fertilization Potential. *Front Cell Dev Biol* 2019; **7**: 230.

12 Brown SG, Publicover SJ, Barratt CLR, Martins da Silva SJ. Human sperm ion channel (dys)function: implications for fertilization. *Hum Reprod Update* 2019; **25**: 758–776.

13 Freitas MJ, Vijayaraghavan S, Fardilha M. Signaling mechanisms in mammalian sperm motility. *Biol Reprod* 2017; **96**: 2–12.

14 Shukla KK, Mahdi AA, Rajender S. Ion Channels in Sperm Physiology and Male Fertility and Infertility. *Journal of Andrology* 2012; **33**: 777–788.

15 Visconti PE, Krapf D, de la Vega-Beltrán JL, Acevedo JJ, Darszon A. Ion channels, phosphorylation and mammalian sperm capacitation. *Asian J Androl* 2011; **13**: 395–405.

16 Dey S, Brothag C, Vijayaraghavan S. Signaling Enzymes Required for Sperm Maturation and Fertilization in Mammals. *Front Cell Dev Biol* 2019; **7**: 341.

17 Fuster DG, Alexander RT. Traditional and emerging roles for the SLC9 Na+/H+ exchangers. *Pflugers Arch - Eur J Physiol* 2014; **466**: 61–76.

18 Cooper TG, Noonan E, von Eckardstein S, Auger J, Baker HWG, Behre HM *et al.* World Health Organization reference values for human semen characteristics*‡. *Human Reproduction Update* 2010; **16**: 231–245.

19 Auger J, Jouannet P, Eustache F. Another look at human sperm morphology. *Hum Reprod* 2016; **31**: 10–23.

20 Martinez G, Kherraf Z-E, Zouari R, Fourati Ben Mustapha S, Saut A, Pernet-Gallay K *et al.* Whole-exome sequencing identifies mutations in FSIP2 as a recurrent cause of multiple morphological abnormalities of the sperm flagella. *Human Reproduction* 2018; **33**: 1973–1984.

21 Martinez G, Beurois J, Dacheux D, Cazin C, Bidart M, Kherraf Z-E *et al.* Biallelic variants in *MAATS1* encoding CFAP91, a calmodulin-associated and spoke-associated complex protein, cause severe astheno-teratozoospermia and male infertility. *J Med Genet* 2020; **57**: 708–716.

22 Lorès P, Dacheux D, Kherraf Z-E, Nsota Mbango J-F, Coutton C, Stouvenel L *et al.* Mutations in TTC29, Encoding an Evolutionarily Conserved Axonemal Protein, Result in Asthenozoospermia and Male Infertility. *Am J Hum Genet* 2019; **105**: 1148–1167.

23 Alpha Scientists in Reproductive Medicine and ESHRE Special Interest Group of Embryology, Balaban B, Brison D, Calderon G, Catt J, Conaghan J *et al.* The Istanbul consensus workshop on embryo assessment: proceedings of an expert meeting. *Human Reproduction* 2011; **26**: 1270–1283.

24 Wang G, Guo Y, Zhou T, Shi X, Yu J, Yang Y *et al.* In-depth proteomic analysis of the human sperm reveals complex protein compositions. *Journal of Proteomics* 2013; **79**: 114–122.

25 Wang D, King SM, Quill TA, Doolittle LK, Garbers DL. A new sperm-specific Na+/H+ Exchanger required for sperm motility and fertility. *Nat Cell Biol* 2003; **5**: 1117–1122.

26 Windler F, Bönigk W, Körschen HG, Grahn E, Strünker T, Seifert R *et al.* The solute carrier SLC9C1 is a Na+/H+-exchanger gated by an S4-type voltage-sensor and cyclic-nucleotide binding. *Nat Commun* 2018; **9**: 2809.

27 Wang D, Hu J, Bobulescu IA, Quill TA, McLeroy P, Moe OW *et al.* A sperm-specific Na+/H+ exchanger (sNHE) is critical for expression and in vivo bicarbonate regulation of the soluble adenylyl cyclase (sAC). *Proceedings of the National Academy of Sciences* 2007; **104**: 9325–9330.

28 Bell SM, Schreiner CM, Schultheis PJ, Miller ML, Evans RL, Vorhees CV *et al.* Targeted disruption of the murine *Nhe1* locus induces ataxia, growth retardation, and seizures. *American Journal of Physiology-Cell Physiology* 1999; **276**: C788–C795.

29 Chen S-R, Chen M, Deng S-L, Hao X-X, Wang X-X, Liu Y-X. Sodium–hydrogen exchanger NHA1 and NHA2 control sperm motility and male fertility. *Cell Death Dis* 2016; **7**: e2152.

30 Nishigaki T, José O, González-Cota AL, Romero F, Treviño CL, Darszon A. Intracellular pH in sperm physiology. *Biochemical and Biophysical Research Communications* 2014; **450**: 1149–1158.

31 Martins AD, Bernardino RL, Neuhaus-Oliveira A, Sousa M, Sá R, Alves MG *et al.* Physiology of Na+/H+ Exchangers in the Male Reproductive Tract: Relevance for Male Fertility1. *Biology of Reproduction* 2014; **91**. doi:10.1095/biolreprod.114.118331.

32 Chávez JC, Ferreira JJ, Butler A, De La Vega Beltrán JL, Treviño CL, Darszon A *et al.* SLO3 K^+ Channels Control Calcium Entry through CATSPER Channels in Sperm. *J Biol Chem* 2014; **289**: 32266–32275.

33 Lishko PV, Botchkina IL, Fedorenko A, Kirichok Y. Acid Extrusion from Human Spermatozoa Is Mediated by Flagellar Voltage-Gated Proton Channel. *Cell* 2010; **140**: 327–337.

34 Berger TK, Fußhöller DM, Goodwin N, Bönigk W, Müller A, Dokani Khesroshahi N *et al.* Post-translational cleavage of Hv1 in human sperm tunes pH- and voltage-dependent gating: Hv1Sper in human sperm. *J Physiol* 2017; **595**: 1533–1546.

35 Romero F, Nishigaki T. Comparative genomic analysis suggests that the sperm-specific sodium/proton exchanger and soluble adenylyl cyclase are key regulators of CatSper among the Metazoa. *Zoological Lett* 2019; **5**: 25.

36 Vyklicka L, Lishko PV. Dissecting the signaling pathways involved in the function of sperm flagellum. *Current Opinion in Cell Biology* 2020; **63**: 154–161.

37 Zhang Z, Yang Y, Wu H, Zhang H, Zhang H, Mao J *et al.* Sodium-Hydrogen-Exchanger expression in human sperm and its relationship with semen parameters. *J Assist Reprod Genet* 2017; **34**: 795–801.

38 Yeung CH, Anapolski M, Depenbusch M, Zitzmann M, Cooper TG. Human sperm volume regulation. Response to physiological changes in osmolality, channel blockers and potential sperm osmolytes. *Human Reproduction* 2003; **18**: 1029–1036.

39 Avidan N, Tamary H, Dgany O, Cattan D, Pariente A, Thulliez M *et al.* CATSPER2, a human autosomal nonsyndromic male infertility gene. *Eur J Hum Genet* 2003; **11**: 497–502.

40 Dirami T, Rode B, Jollivet M, Da Silva N, Escalier D, Gaitch N *et al.* Missense Mutations in SLC26A8, Encoding a Sperm-Specific Activator of CFTR, Are Associated with Human Asthenozoospermia. *The American Journal of Human Genetics* 2013; **92**: 760–766.

41 Wedenoja S, Khamaysi A, Shimshilashvili L, Anbtawe-Jomaa S, Elomaa O, Toppari J *et al.* A missense mutation in SLC26A3 is associated with human male subfertility and impaired activation of CFTR. *Sci Rep* 2017; **7**: 14208.

42 Asmarinah, Nuraini T, Sumarsih T, Paramita R, Saleh MI, Narita V *et al.* Mutations in exons 5, 7 and 8 of the human voltage-dependent anion channel type 3 (VDAC3) gene in sperm with low motility: VDAC3 gene mutations in low motile sperm. *Andrologia* 2012; **44**: 46–52.

43 Liu W, Xie Y, Ma J, Luo X, Nie P, Zuo Z *et al.* IBS: an illustrator for the presentation and visualization of biological sequences: Fig. 1. *Bioinformatics* 2015; **31**: 3359–3361.

44 Ren J, Wen L, Gao X, Jin C, Xue Y, Yao X. DOG 1.0: illustrator of protein domain structures. *Cell Research* 2009; **19**: 271–273.

	General Semen Characteristics						Flagellar defects					Midpiece defects	Head defects		Acrosome defects	
	Volume (ml)	Sperm concentration (10^6/mL)	Total Motility	Progressive Motility	Vitality	Typical forms	Absent	Short	Irregular	Coiled	Bent	Excess residual cytoplasm	Tapered	Thin	Post-acrosomal	Acrosomal
	3.9	117.5	**25**	**5**	**49**	26	1	1	1	5	**19**	**14**	0	3	**53**	35
	3.4	52	**30**	**5**	62	23	ND	ND	ND	ND	ND	ND	ND	ND	ND	ND
	3.5	74	**35**	**5**	82	**10**	3	**3**	0	5	10	1	3	**36**	22	**78**
	2.4	73	**15**	**0**	80	**15**	0	2	0	3	6	**10**	2	**25**	45	**80**
	3.8	103	**25**	**5**	67	ND	ND	ND	ND	ND	ND	ND	ND	ND	ND	ND
mean	3.4	83.9	**26**	**4**	68	**18.5**	1.3	2	0.3	4.3	11.6	**8.3**	1.7	**21.3**	40	**64.3**
Reference limits [a]	1.5 (1.4-1.7)	15 (12-16)	40 (38-42)	32 (31-34)	58 (55-63)	23 (20-26)	5 (4-6)	1 (0-2)	2 (1-3)	17 (15-19)	13 (11-15)	4 (3-5)	3 (2-4)	14 (12-16)	42 (39-45)	60 (57-63)

Table 1 – Semen parameters and sperm morphological defects (flagellum, head and acrosome) of the patient carrying a mutation in *SLC9C1* gene Five semen evaluations were performed for the patient over 3 years. Values are expressed in percent, unless specified otherwise. ND: not determined.

[a] Lower or upper reference limits (5th centiles and their 95% confidence intervals) according to the World Health Organization (WHO) standards and the distribution range of morphologically abnormal spermatozoa observed in fertile individuals[18,19]; in bold characters: abnormal values.

Figures

Figure 1

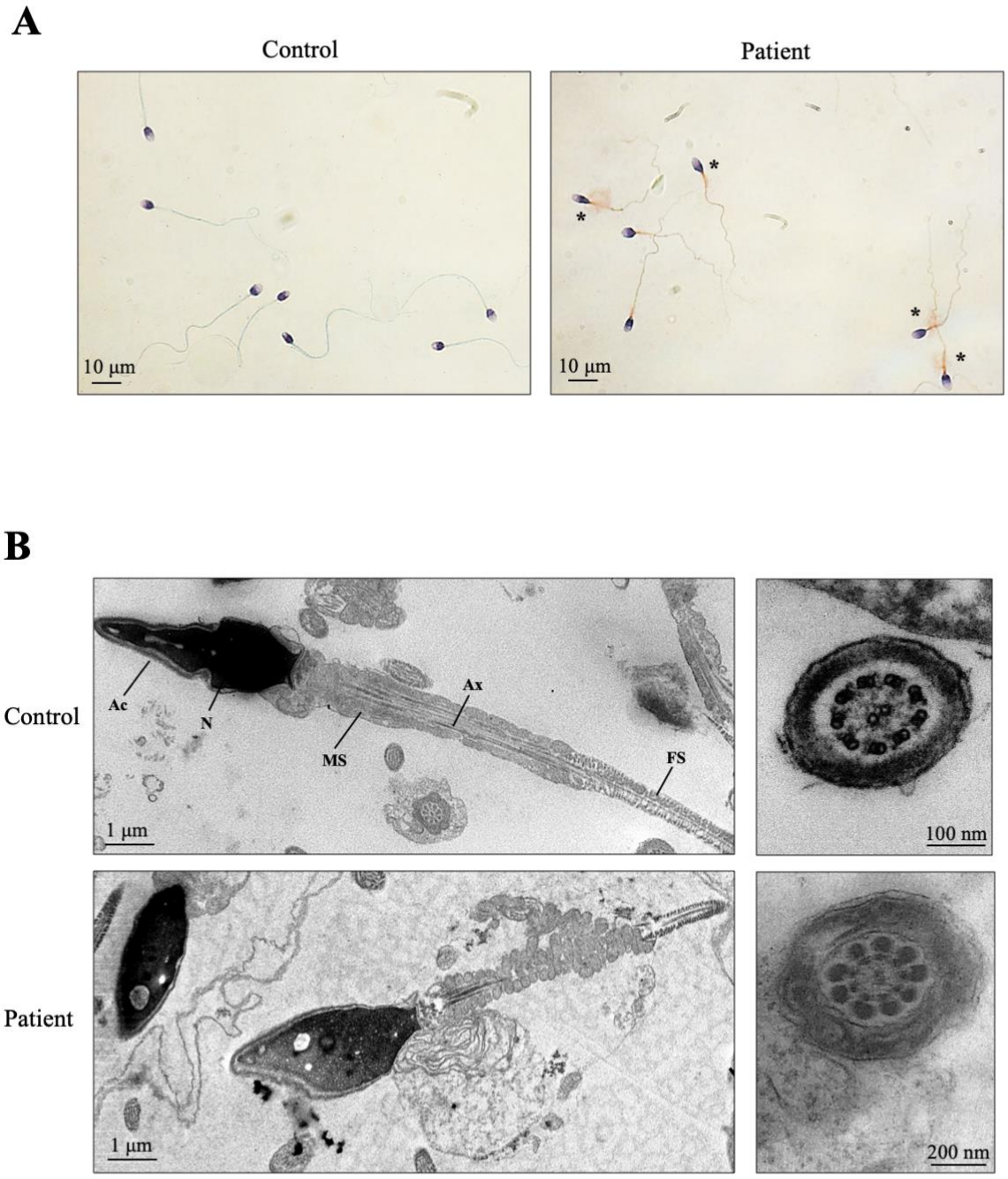

Figure 1 – Morphological and ultrastructural anomalies of spermatozoa from the patient.

(A) Morphology of spermatozoa from the patient (right) compared to spermatozoa from a control individual (left). Semen analysis showed a fraction of spermatozoa carrying disorganised midpiece with residual cytoplasm and plasma membrane lysis (*****). Scale bars represent 10 μm. (B) Transmission Electron Microscopy analysis of semen sample from a control individual (top) and from the patient (bottom), showing flagellar longitudinal and transversal sections. Spermatozoa from the patient showed residual cytoplasm associated with plasma membrane lysis and irregular mitochondrial sheath. The transversal sections of spermatozoa from the patient showed normal ultra-structure with the (9+2) pattern. Scale bars represent 1μm, 100 and 200 nm. *Ac, acrosome; N, nucleus; MS, mitochondrial sheath; Ax, axoneme; FS, fibrous sheath.*

Figure 2

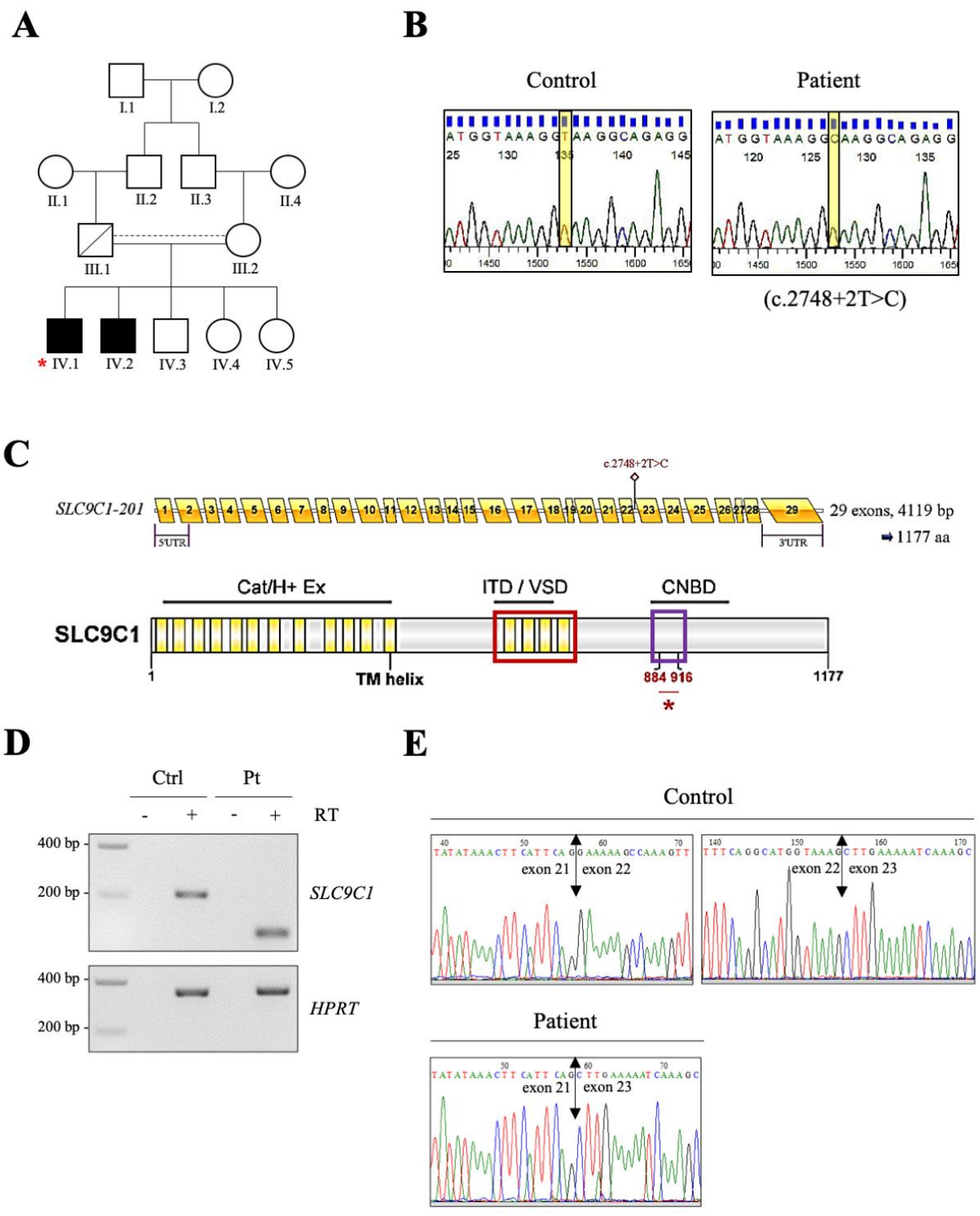
A
I.1
I.2
II.1
II.2
II.3
II.4
III.1
III.2
* IV.1
IV.2
IV.3
IV.4
IV.5
B
Control
Patient
(c.2748+2T>C)
C
c.2748+2T>C
SLC9C1-201
29 exons, 4119 bp
1177 aa
5'UTR
3'UTR
Cat/H+ Ex
ITD / VSD
CNBD
SLC9C1
TM helix
884 916
1177
D
Ctrl
Pt
RT
400 bp
200 bp
SLC9C1
HPRT
E
Control
exon 21
exon 22
exon 23
Patient

Figure 2 – Pedigree of the patient, description of the *c.2748+2T>C* mutation in *SLC9C1* and analysis of the transcript in sperm from the patient.

(A) Pedigree of the infertile patient with functional asthenozoospermia. The proband (IV.1) is indicated by the red asterisk. Consanguinity between parents (III.1 and III.2) is indicated by the dashed line. One of the brothers of the proband (IV.2) is also known to be infertile; the second one (IV.3) has not manifested desire of parenthood yet. The two sisters of the proband (IV.4 – IV.5) are fertile and had children. A cousin not illustrated in the pedigree was also reported by the proband to be infertile. (B) Electropherograms of *SLC9C1* Sanger sequencing for patient and control individual. The *c.2748+2T>C SLC9C1* mutation identified by WES was confirmed by Sanger sequencing. (C) (top) Linear structure of *SLC9C1* main transcript (*SLC9C1-201*) showing the exons (yellow boxes), according to the gene description available from Ensembl database. The localization of the mutation is pointed by a stick [figure obtained with IBS tool of DOG software[43]]. (bottom) Linear structure of SLC9C1 protein (SLC9C1-201 isoform). The yellow boxes represent transmembrane (TM) helices and the horizontal bars indicate all functional domains: Cat/H^+ Ex, Cation/H^+ Exchanger domain; ITD / VSD, Ion Transport-like Domain / Voltage-Sensing Domain; CNBD, Cyclic Nucleotide-Binding Domain. Red and purple boxes highlight the epitopes of the two antibodies used in the study, the 'Central antibody' and the 'C-Terminal antibody' respectively. The region between amino-acids 884 and 916 is encoded by exon 22 [figure obtained with DOG software[44]]. (D) RT-PCR analysis of a semen sample from the patient carrying the *c.2748+2T>C* mutation. The expected amplicon size is 217 bp for *SLC9C1* transcript and 352 bp for *HPRT*. RNA samples treated in absence of Reverse Transcriptase (- RT) constituted negative experimental controls. (E) Electropherogram of *SLC9C1* transcript sequencing for a control individual and the patient. In the sample from the patient, sequencing indicates the absence of exon 22 due to the *c.2748+2T>C* mutation, which abrogates intron 22 splice donor site.

Figure 3

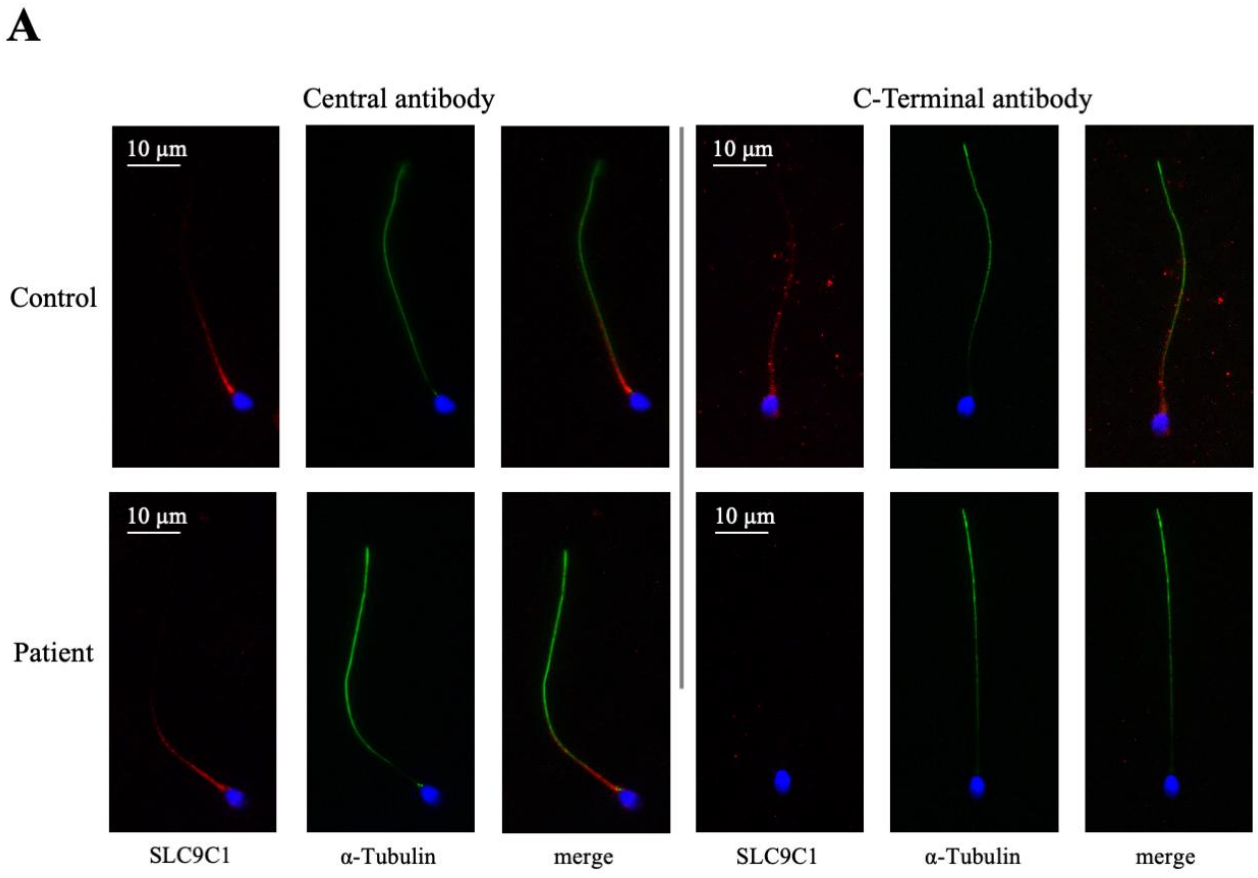
A
Central antibody
C-Terminal antibody
10 µm
Control
Patient
SLC9C1
α-Tubulin
merge
B
Ctrl
Pt
130 kDa
55 kDa
SLC9C1
β-Tubulin

Figure 3 – Analysis of SLC9C1 protein in sperm from the patient carrying the *c.2748+2T>C* mutation.

(A) SLC9C1 protein detection (red) by immunofluorescence assay in sperm cells from control individual (top) and patient (bottom). Two different antibodies were used: one antibody directed against the central region of SLC9C1 and a second antibody directed against the C-Terminal region and including exon 22 coding region. Co-staining with α-Tubulin antibody (green) was also performed. The protein localises at the midpiece and principal piece of sperm flagella, with a decreasing gradient towards the end of the tail. The Central antibody allowed to confirm presence of SLC9C1 in patient spermatozoa, while absence of signal of the C-Terminal antibody confirmed an abnormal protein lacking part of the CNBD. Scale bars represent 10μm. (B) Immunoblotting detection of SLC9C1 protein (135 kDa) in sperm lysate from control individual (left) and patient (right). β-Tubulin (55 kDa) was used for normalization.

Supplementary Data

Figure S1

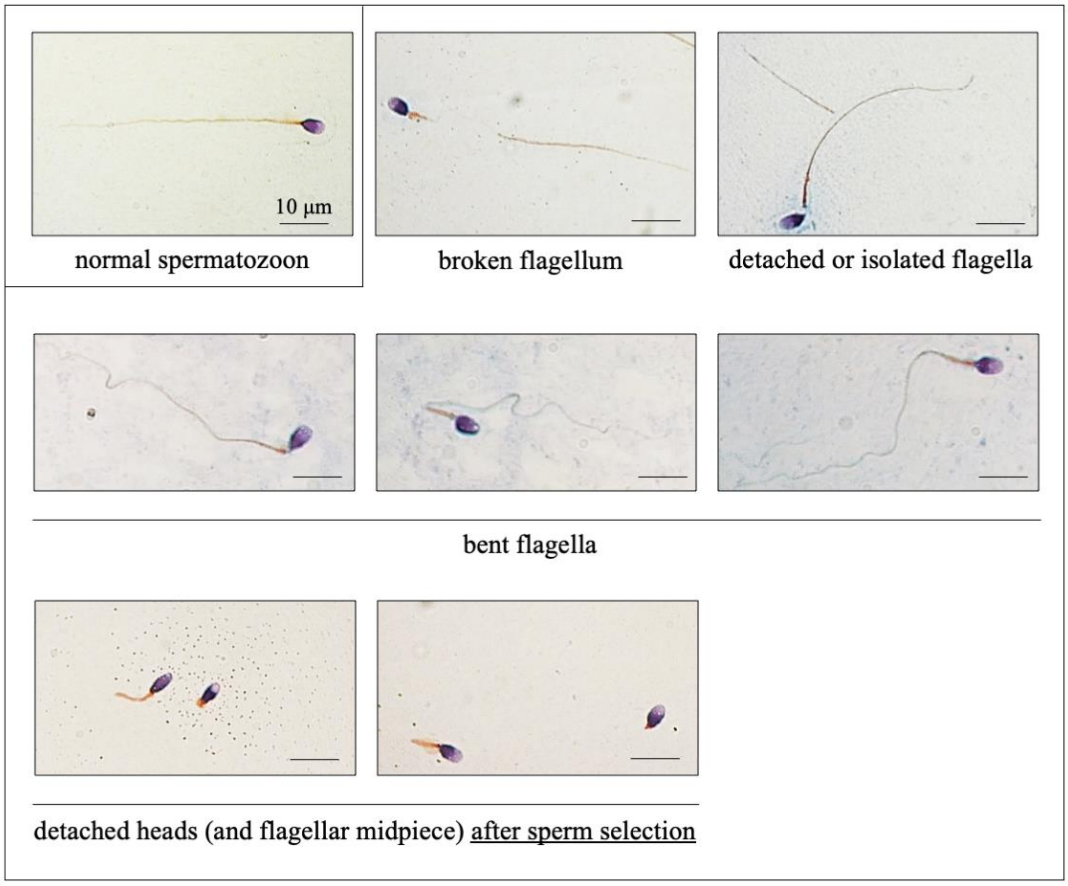

Figure S1 – Details of the flagellar morphological anomalies observed in sperm from the patient.

Catalogue of the sperm flagellar defects observed in semen from the patient carrying the *c.2748+2T>C* mutation, compared to a normal spermatozoon (top, left corner). Various flagellar angulation and break points were observed at the level of the connecting piece or along the flagellum, suggesting a fragility of the sperm tail. This phenotype was even more evident after sperm selection with density gradient centrifugation. Scale bar represents 10 µm.

Figure S2

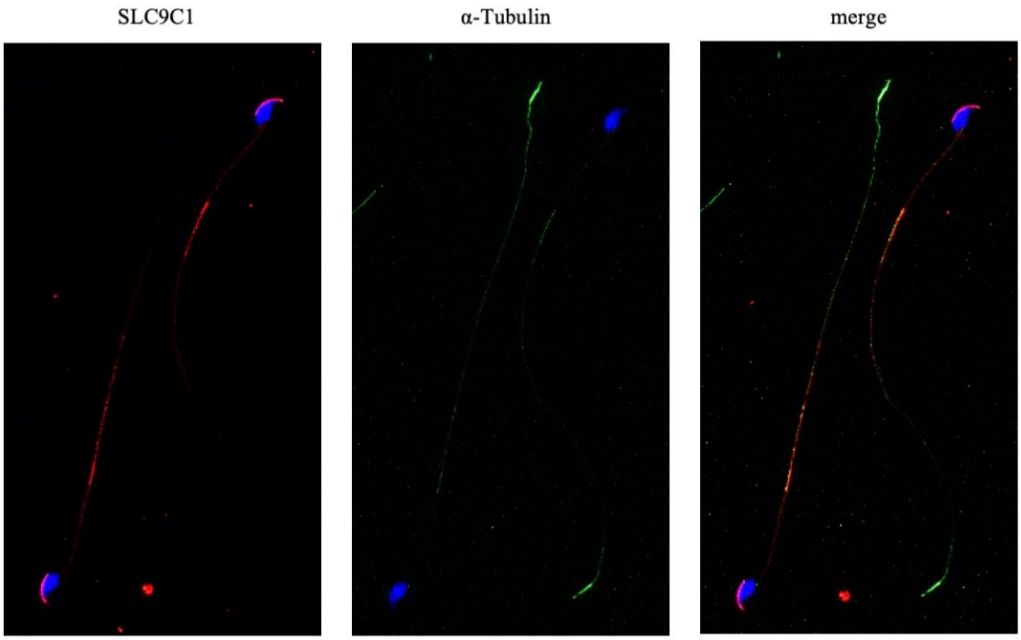

Figure S2 – SLC9C1 detection in mouse spermatozoa.

Immunofluorescence detection of SLC9C1 protein on mouse spermatozoa using the antibody directed against the central region of SLC9C1, co-staining with α-Tubulin (green). SLC9C1 (red) preferentially localises at the principal piece of the flagella. Scale bar represents 10μm.

Gene	Testis/all tissue gene expression ratio	Variant	Frequency (gnomAD database)	Nature of the variant	Predicted effect at protein level	Detection in sperm proteome (Wang *et al.*, 2013)
SLC9C1	12.71	c.2748+2T>C	$4.576\ 10^{-5}$	Splice donor variant	-	+
ABCB5	2.37	c.3583C>T	0.0008645	Stop gained	p.Gln1195Ter	-
ZNF891	1.71	c.9del	0.003403	Frameshift variant	p.Met4TrpfsTer9	-

Supplementary Table 1 – Homozygous variants with high pathogenic impact proposed for the patient by bioinformatic analysis of WES data.